PHYSICAL REVIEW B VOLUME 26, NUMBER 8 15 OCTOBER 1982

Absorption-edge resonances, core-hole screening, and orientation of chemisorbed molecules: CO, NO, and N_2 on Ni(100)

J. Stöhr and R. Jaeger
Corporate Research Science Laboratories, Exxon Research and Engineering Company, Linden, New Jersey 07036
(Received 10 May 1982)

Near-edge x-ray-absorption fine-structure spectra are reported above the K absorption edges of diatomic low-Z molecules (CO, NO, and N_2) chemisorbed on Ni(100). It is shown that the K-edge fine structure is dominated by intramolecular resonances which arise from a sharp bound-state transition to an unoccupied molecular orbital of π symmetry and a broader σ shape resonance in the continuum. For dissociated molecules the K absorption-edge structure is found to be distinctly different, and large (~ 3 eV) shifts of the edge position are observed. The position of the molecular resonances is discussed in comparison with gas-phase absorption data and the $1s$ binding energies determined by photoemission. The question of ligand 2π and metal d charge transfer is discussed for the neutral and ionic (core-hole) chemisorption complex. For N_2 on Ni(100) the giant satellite structure in the N $1s$ photoemission spectrum due to dynamic screening of the core hole has been measured at $h\nu = 500$ eV, and comparison is made with the absorption case. A theoretical expression is derived for the polarization dependence of the resonance structures which allows the precise determination of the molecular orientation on the surface. Comparison is made to the theory governing angle-resolved photoemission spectra. The molecular orientation for CO, NO, and N_2 on Ni(100) at saturation coverage is determined. All molecules are found to stand up on the surface with the molecular axis along the surface normal ($\pm 10°$).

I. INTRODUCTION

Core-electron excitation spectra of gas-phase molecules have been studied for many years by photoabsorption measurements using bremsstrahlung[1-3] or synchrotron radiation[4-7] and by electron energy-loss spectroscopy.[8-11] For all studied molecules ranging from di- to polyatomic sizes, it is found that the region around the K $1s$ absorption threshold is dominated by resonance structures of varying energy position, width, and intensity. The position of the most pronounced resonance(s) always corresponds to an excitation energy which is less ($\sim 5-10$ eV) than the $1s$ ionization energy (i.e., the binding energy relative to the vacuum level). Such *"bound-state resonances"* originate from transitions to a partially filled molecular orbital or an unfilled orbital which is pulled below the vacuum level by the Coulomb interaction with the created core hole. Above the ionization threshold (< 10 eV) other broader resonances are typically observed. These latter *"shape resonances"* were first explained by Dehmer and Dill[12,13] for diatomic molecules as a relative increase in the amplitude of a continuum state of σ symmetry near the molecule.

The presence and properties of the σ shape resonance have since then received considerable attention in valence- and core-level photoemission studies of gas-phase[14] and chemisorbed[15-18] molecules. In particular, the symmetry properties of electronic excitations from σ or π initial states to the σ shape resonance have been exploited in polarization-dependent angle-resolved photoemission spectroscopy (PARPES) studies to determine the molecular orientation on the surface. Recently it has been shown that, just as in the gas phase, the K-absorption thresholds for chemisorbed molecules are also dominated by bound-state and continuum-resonance structures.[19] For chemisorbed molecules the absorption coefficient can be obtained by measurement of the Auger electron yield corresponding to filling of the K-shell vacancy after photon absorption.[19-23] Such near-edge x-ray-absorption fine-structure (NEXAFS) spectra exhibit a strong polarization dependence because the resonance peak intensities are governed by $\sigma \rightarrow \pi$ or $\sigma \rightarrow \sigma$ dipole transitions. In particular, the narrow and stronger bound-state transitions which are not observable in photoemission show the largest polarization effects since the final-state molecular orbitals are of pure

symmetry and the resonance peaks ride on a structureless background. Thus their *intensity* variation as a function of the electric field vector ($\vec{E}$) orientation of the photon beam is a sensitive measure of the molecular orientation on the surface. In contrast to PARPES studies, NEXAFS measurements depend only on the $\vec{E}$ vector orientation with respect to the sample.

For diatomic molecules, such as CO, NO, or N_2 which are chemisorbed on *d* band metals, the *K*-edge absorption spectra are dominated by a bound-state transition to an antibonding orbital of π symmetry. This orbital is formed from the unfilled or partially filled 2π molecular orbital and substrate *d* states of π symmetry. The *intensity* of this transition may be expected to be correlated with the details of the metal (*d*) to molecule (2π) charge transfer which has been the subject of much discussion in the literature.[24–27] As suggested by Blyholder[24] such a charge transfer decreases the intramolecular bond strength leading to an increase of the bond length and to a softening of the intramolecular stretching mode.[28] Also, it is believed that the π final-state orbital which gives rise to the bound-state transition plays an important role in the core-hole screening process[29] (shake-down[30]) or in multielectron (shake-up) excitations[31,32] in photoemission. The peak *positions* of the resonances also provide valuable information. As discussed by Bianconi *et al.*[33] a change in intramolecular bond length should lead to a different separation between the two final-state resonances. Furthermore, the position of the *K*-absorption threshold and the edge fine structure can be used to readily distinguish between molecular versus atomic (dissociative) chemisorption.

It is the purpose of this paper to discuss experimental and theoretical details of NEXAFS measurements. Using CO, NO, and N_2 chemisorption on Ni(100) as examples, we demonstrate the potential of the technique for the investigation of electronic properties and the geometry of chemisorbed molecules. Throughout the paper close contact is kept with the physical processes and the theory underlying angle-resolved valence- and core-level photoemission.

The structure of the paper is as follows. Section II discusses experimental details of NEXAFS measurements and Sec. III gives experimental results for CO, NO, and N_2 on Ni(100). A comparative discussion of photoemission core-electron binding energies and the position of absorption-edge resonances is presented in Sec. IV. Section V deals with theoretical aspects of polarization-dependent angle-resolved photoemission and polarization-dependent NEXAFS measurements of chemisorbed molecules. In Sec. VI we discuss the determination of the molecular orientation for the three investigated chemisorption systems by NEXAFS. The paper concludes in Sec. VII with a summary of the results and a future outlook.

II. EXPERIMENTAL

A. Experimental arrangement

Experiments were carried out on the grasshopper monochromator[34] on beam line I at the Stanford Synchrotron Radiation Laboratory (SSRL). The monochromator was equipped with a freshly coated 1200 lines/mm holographic grating. The experimental geometry is shown in Fig. 1. As discussed before[35] the incident photon beam intensity is monitored by collecting the total electron yield (TEY) from a high-transmission metal grid which for the present studies was freshly coated with copper. The TEY signal amplified by a high-current channeltron electron multiplier (CEM) is used to normalize the Auger electron yield (AEY) from the sample to any fluctuations or $h\nu$-dependent modulations of the monochromatic beam intensity.[35] The sample is rotatable about a vertical axis and positioned in the focal point of a cylindrical-mirror electron energy analyzer (CMA). The symmetry axis of the CMA lies in the horizontal plane parallel to the $\vec{E}$ vector of the incident photon beam. The CMA is equipped with an internal electron gun allowing Auger surface characterization. A high-current CEM close to the sample may be used for TEY measurements. The vacuum chamber with a base pressure in the low 10^{-10}-Torr range is of dual-level design with a low-energy electron diffraction

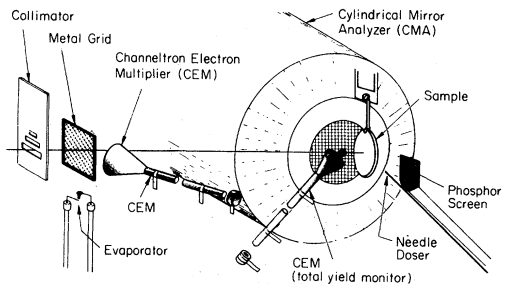

FIG. 1. Experimental arrangement for Auger and total electron yield NEXAFS measurements.

(LEED) optics, ion sputter gun, and residual gas analyzer on the upper level.

The Ni(100) single crystal (~0.6-in. diameter) was mounted on a thin sheet (~0.005-in. thickness) of Ta metal which was coupled to a liquid-nitrogen reservoir by a short copper block and a thin sapphire disc. The sample could be heated from behind by electron bombardment from a W filament. This arrangement allowed cooling down to 90 K and heating to at least 1300 K as verified by a Chromel-Alumel thermocouple. The Ni(100) crystal was cleaned by Ar^+ sputtering and oxygen or NO heat treatments to produce a surface with less than 1% of C, O, and S. The clean annealed surface was characterized by Auger electron spectroscopy and LEED. NEXAFS spectra were recorded after dosing the clean surface to saturation coverage with CO, NO, or N_2. Exposures [20 L (1 L=1 Langmuir=10^{-6} Torr sec) at 5×10^{-7} Torr] and measurements for CO were carried out over the 90–300 K temperature range. For NO and N_2 the exposure (20 L) and measurement temperature was 90 K.

B. Energy calibration and flux normalization

In order to accurately measure the energy position of absorption structures the monochromator output energy needs to be calibrated. For solids, core-electron binding energies relative to the Fermi level are accurately known from photoemission. For a metal the absorption edge corresponds to an electronic transition to the Fermi level. Thus the monochromator is calibrated by aligning the inflection point of a prominent absorption edge (assuming that the monochromator broadening function is Gaussian) with the corresponding inner-shell binding energy. Often the L_3 edge positions of Al (72.7±0.2 eV) (Ref. 36) or Si (99.8±0.2 eV) (Ref. 37) are used in the vacuum ultraviolet range and those of the 3*d* transition metals[38] Ti (454 eV) through Ni (853 eV) in the soft x-ray region. Unfortunately, published binding energies often differ significantly[38] and thus calibration of the monochromator is a nontrivial matter. Figure 2 shows the TEY spectrum of Ni metal around the L_3 edge which was used to calibrate the monochromator. The calibration was checked at the *K* edges of chemisorbed C, N, and O atoms on Ni(100). Results from photoemission and absorption (inflection point of edge) measurements are compared in Table I. From these data we believe the *absolute* photon energy scale to be correct to better than 0.5 eV in the (250–600)-eV spectral range used here. This energy uncertainty lies within the energy resolution of the monochromator.[34,35]

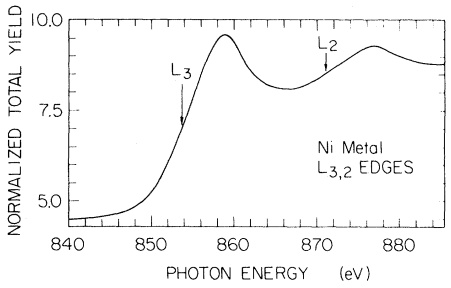

FIG. 2. Ni L_3 and L_2 edges for clean Ni(100) recorded with the grasshopper monochromater (1200 lines/mm grating) in the total electron yield mode.

The problems associated with normalization of structures in the monochromator transmission function have been discussed previously.[35,39] The C *K*-edge region is most problematic because it exhibits the largest flux modulations as shown in Fig. 3. Both the TEY reference signal from the clean Cu grid (I_0) as well as the AEY from the clean Ni(100) sample (I) exhibit a large signal loss (about a factor of 2) between 280 and 310 eV with two minima at 284.7 and 291.0 eV. This structure has been shown to be due to the "white line" absorption of carbon contamination on the optical surfaces of the beam line.[39] It is, however, almost completely (<3% modulation) normalized out in the ratio I/I_0 of the two signals. Figure 3 represents the worst normalization conditions dealt with in the present experiments and was recorded with the same C *KVV* Auger window (E_k=263 eV) setting as for the CO on Ni(100) case discussed below.

TABLE I. Photoemission 1*s* binding energies and *K*-absorption edge positions for C, N, and O on Ni(100).

Atom on Ni(100)	Hole state	PES E_B (eV)	Edge[d] E_A (eV)
C	1*s*	282.5±0.2[a]	283.0±0.5
N	1*s*	397.8±0.2[b]	397.5±0.5
O	1*s*	529.5±0.2[c]	529.8±0.5

[a]C. R. Brundle (private communication) for dissociated CO.
[b]C. R. Brundle, J. Vac. Sci. Technol. 13, 301 (1976), for dissociated NO on polycrystalline Ni.
[c]C. R. Brundle, in *Aspects of the Kinetics and Dynamics of Surface Reactions,* edited by U. Landman (AIP, New York, 1980), for $c(2\times2)$O on Ni(100).
[d]Inflection point of edge.

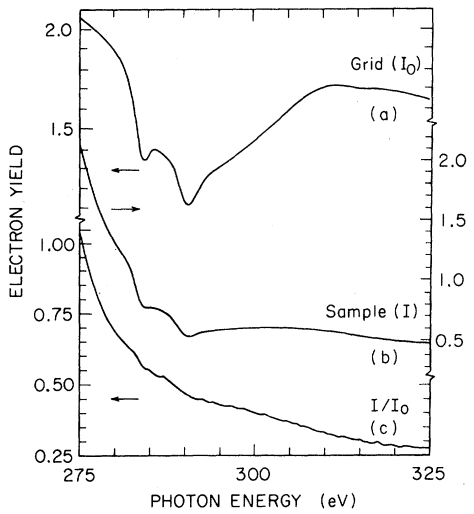

FIG. 3. Monochromator transmission structure around the C K-edge region as revealed by (a) the clean Cu grid reference monitor (I_0) and (b) the clean Ni(100) Auger yield signal (I). (c) The two-peak structure is normalized out when the ratio I/I_0 is taken.

III. EXPERIMENTAL RESULTS

A. Measurement technique

Auger electron spectra of the C, N, and O KVV transitions for CO and NO on Ni(100) are shown in Fig. 4. The spectra were recorded with the CMA (resolution 1.6 eV) at the indicated photon energies about 15 eV above the respective K thresholds. In all cases, the Auger spectra are composed of various peaks similar to x-ray excited gas-phase[40] and adsorbate[41] spectra and fall between the Ni valence-band (VB) and Ni $3p$ photoemission peaks.

Auger yield NEXAFS spectra are recorded by positioning the CMA energy window on the peak of a particular Auger transition (i.e., C: 263 eV, N: 379 eV, O: 511 eV) and measuring the strength of this Auger signal as a function of $h\nu$ around the corresponding absorption edge. In order to obtain maximum signal, the CMA was operated in the nonretarding mode[42] yielding an energy resolution of ~ 4, ~ 6, and ~ 8 eV at the C, N, and O Auger energies, respectively. The instrumental resolution of the K-edge absorption spectra is, of course, independent of the CMA window width but solely depends on the monochromator energy resolution.

Figure 5 shows Auger yield NEXAFS spectra recorded for two angles of incidence θ, around the O K edge for CO on Ni(100) and for clean Ni(100). As the photon energy is scanned from 500 to 600

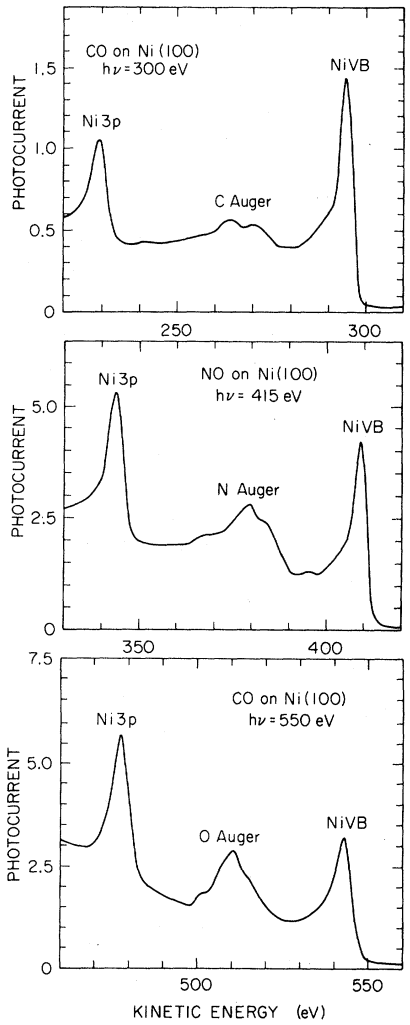

FIG. 4. Ni photoemission spectra and C, N, and O KVV Auger spectra for CO and NO on Ni(100) recorded at a photon energy of ~ 15 eV above the respective K edges.

eV, the Ni VB photoemission peak and the weak molecular valence orbitals (5σ, 1π, and 4σ) are first swept through the fixed Auger window. Around 531 eV, the threshold of the O $1s$ excitation is reached and the O KVV channel is opened up. Two pronounced absorption resonances, A and B, are observed between 530 and 570 eV. These resonances exhibit a strong and opposite polarization dependence. The Ni $3p$ photoemission peak is swept through the Auger window at $h\nu = 580$ eV and thereby limits the usable photon energy range over which the O K-edge absorption fine structure can be studied. As discussed previously for O on Si(111),[23] Auger yield measurements above low-Z K edges can therefore not be employed for extended x-ray-

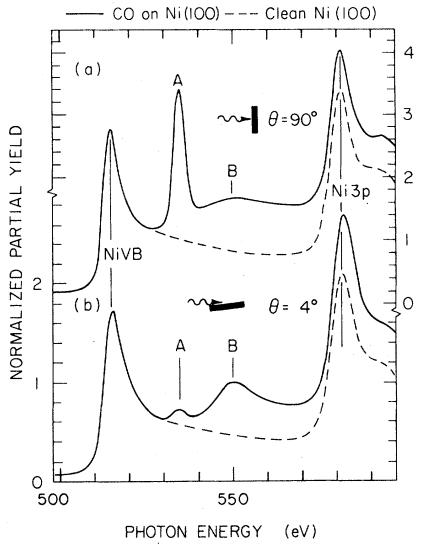

FIG. 5. Normalized O Auger yield spectrum (CMA window at 511 eV) of CO on Ni(100) and clean Ni(100) in the photon energy range 500–600 eV for two angles of x-ray incidence θ.

absorption fine-structure (EXAFS) measurements. The dashed line for clean Ni(100) in Fig. 5 can be used for background subtraction purposes as shown for CO and NO on Ni(100) at an incidence angle $\theta=45°$ in Figs. 6 and 7. In these figures, we have also marked the corresponding C (Ref. 43) and N (Ref. 44) 1*s* binding energies (BE) relative to the Fermi level. In both cases, the BE's coincide within 0.5 eV with the onset energy of the first molecular absorption resonance.

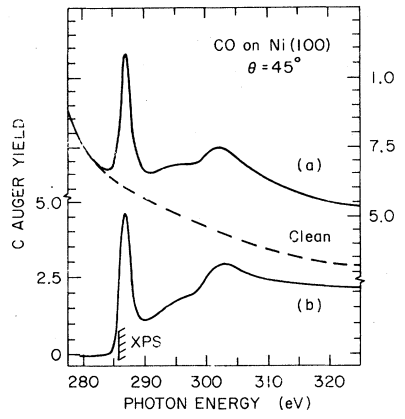

FIG. 6. (a) NEXAFS spectra of the C *K*-edge region for CO on Ni(100) and clean Ni(100) (dashed line) recorded at $\theta=45°$. (b) After subtraction of the dashed from the solid line in (a) to eliminate background. The C 1*s* ionization threshold determined by photoemission is marked XPS.

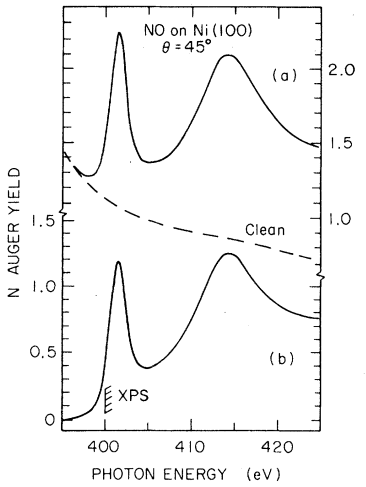

FIG. 7. Same as Fig. 6 for the N *K*-edge region and NO on Ni(100).

B. Molecular versus atomic chemisorption

The sensitivity of the NEXAFS spectra to the structure of the surface complex which is formed during chemisorption is demonstrated by Figs. 8 and 9 for CO and NO on Ni(100), respectively. Figure 8(a) shows the C *K*-edge structure for molecular CO at $\theta=20°$ x-ray incidence. The edge structure changes dramatically upon dissociation of the molecule after heating to 400 °C. The spectrum in Fig. 8(b) is characteristic of atomic C on the surface and corresponds to less than $\frac{1}{2}$ monolayer coverage. This spectrum can also be produced by sputtering of the crystal and subsequent heating such that C segregates to the surface. Therefore, peaks *A* and *B*

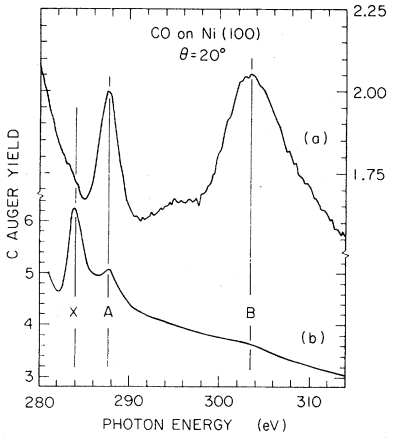

FIG. 8. Comparison of the C *K*-edge NEXAFS spectra for (a) molecular CO on Ni(100), (b) dissociated CO on Ni(100).

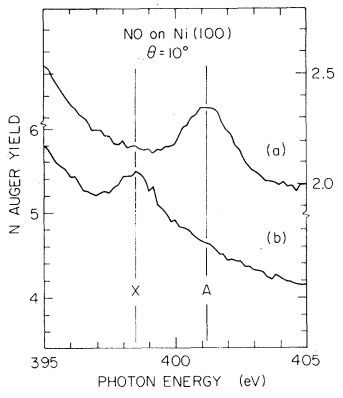

FIG. 9. N K-edge NEXAFS spectra for (a) molecular NO on Ni(100) and (b) dissociated NO on Ni(100).

in Fig. 8(b) are not due to residual CO but rather are EXAFS oscillations due to C-Ni scattering. The most pronounced change is the energy shift of the K-edge position. Peak X falls at 284.0 eV which represents a 3.5-eV shift to lower energy relative to the first peak A for the chemisorbed molecule. This shift is similar to the chemical shift of the C 1s BE in photoemission between dissociated CO (282.5 eV) (Ref. 45) and molecular CO (285.6 eV) (Ref. 45) on Ni(100).

Results for undissociated and dissociated NO on Ni(100) are shown in Figs. 9(a) and 9(b), respectively. Figure 9(a) corresponds to saturation NO coverage (Fig. 13 below) and Fig. 9(b) was recorded after heating to 500 °C and represents a small fraction of a monolayer of atomic N on Ni(100). The shift between the first absorption peaks X at 398.5 eV and A at 401.2 eV is comparable to that observed for CO. The corresponding N 1s binding energies on polycrystalline Ni are 397.8 eV (dissociated NO) (Ref. 45) and 399.9 eV (molecular NO).[44] It can be concluded from these results that NEXAFS can be used as a very sensitive "fingerprint" technique to detect changes in surface structure. This fact has been exploited before to study the oxidation of Al (Refs. 46 and 47) and Si(111) (Refs. 35 and 48) surfaces above the substrate $L_{2,3}$ absorption edge and O K edge.

C. Molecular NEXAFS spectra

1. CO on Ni(100)

Experimental spectra around the C K-edge region for CO on Ni(100), are shown in Fig. 10 for various incidence angles θ of the x-rays from the surface. Similar spectra for the O K edge are shown in Figs. 11 and 12 before and after background subtraction (compare Figs. 6 and 7), respectively. For both

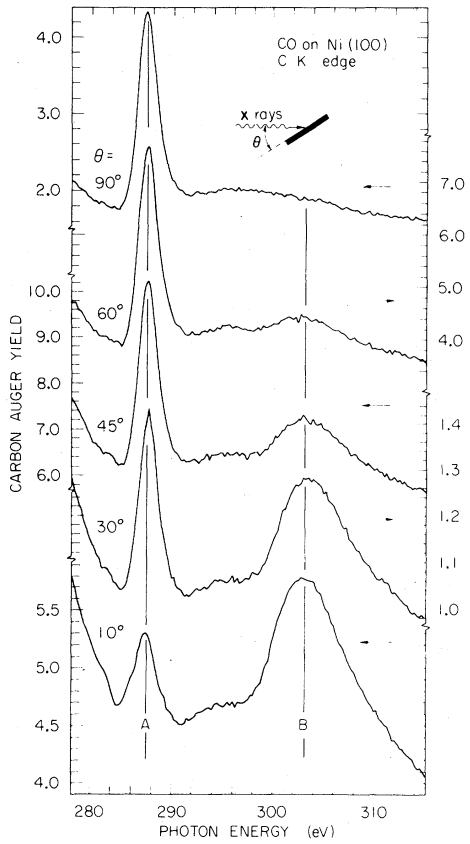

FIG. 10. NEXAFS spectra above the C K edge for CO on Ni(100) at $T=180$ K as a function of incidence angle θ.

edges, the spectra at normal incidence ($\theta=90°$) are dominated by a strong and narrow absorption structure A. Peak A occurs at 287.5 eV with a full width at half maximum (FWHM) of 2.1 eV and at 534.0 eV with FWHM of 3.7 eV, respectively. At grazing incidence ($\theta=10°$) peak A has almost vanished and peak B dominates. This broader peak is centered around 303.0 and 550.0 eV, respectively. At intermediate angles, a gradual transition between the two extremes is observed.

For the C K edge (Fig. 10) a low-energy shoulder of peak B is observed which at some incidence angles (e.g., $\theta=60°$) has the appearance of another peak. The resonance B disappears completely at $\theta=90°$ for the C K edge but seems to be still observable for the O K edge. The measured spectra were identical within the investigated temperature range 90–300 K.

2. NO on Ni(100)

The NEXAFS spectra around the N and O K edges for NO on Ni(100) are shown in Figs. 13 and

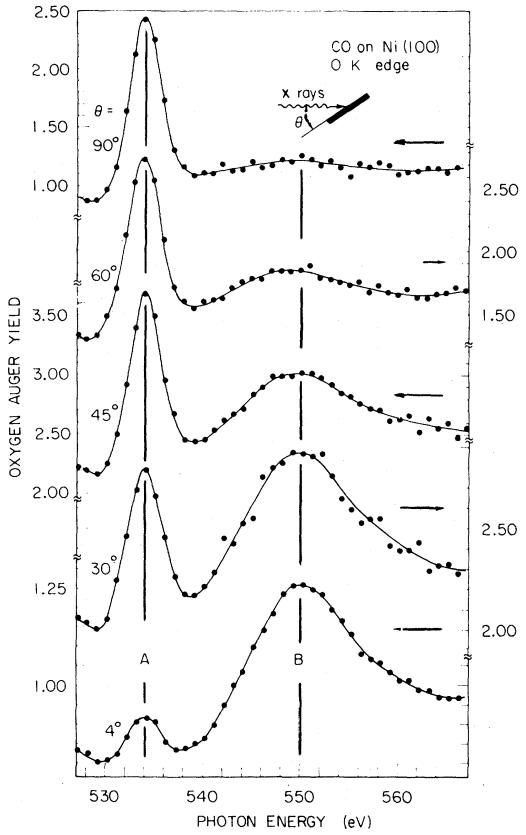

FIG. 11. Same as Fig. 10 above the O K edge.

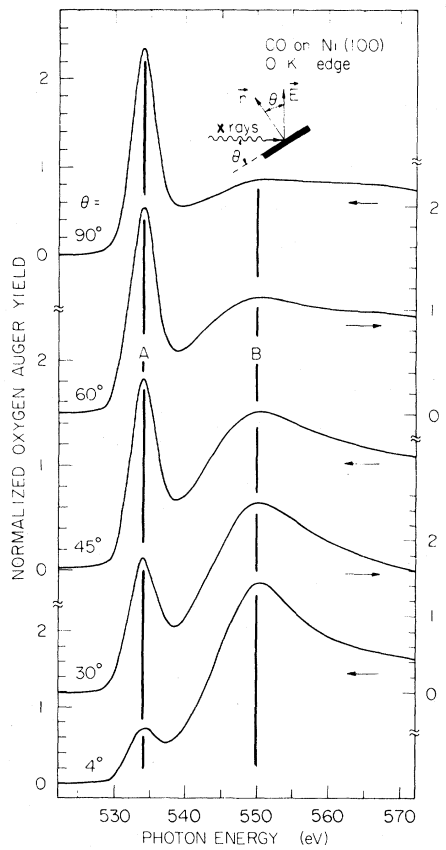

FIG. 12. Background subtracted NEXAFS spectra for CO on Ni(100) above the O K edge.

14, respectively. The spectra and polarization dependence are similar as for CO on Ni(100). Peaks A occur at 401.5 and 534.0 eV with FWHM of 2.4 and 3.7 eV, respectively. Peaks B fall at 414.5 and 546.0 eV and thus are about 3—4 eV closer to peak A than for CO. For the N K edge (Fig. 13), it appears at first sight as if peak B does not vanish at normal x-ray incidence. However, closer inspection reveals that the remaining structure is shifted by ~ 2 eV to lower $h\nu$. As for CO peak B remains finite for $\theta = 90°$ above the O K edge. Peak B is stronger relative to peak A for NO than for CO on Ni(100).

3. N_2 on Ni(100)

The resonances at the N K edge for N_2 on Ni(100) are shown in Fig. 15. Again, the two resonances A and B exhibit a similar polarization dependence as for CO and NO. Peak A falls at 401.0 eV with a FWHM of 2.4 eV and peak B is centered at 418.5 eV. This latter peak completely vanishes at normal x-ray incidence ($\theta = 90°$).

As indicated in Figs. 6 and 7, the onset of peak A for CO and NO on Ni(100) coincides very closely with the respective 1s binding energy positions relative to the Fermi level as determined by photoemission.[43,44] Whereas the 1s core spectra for these latter chemisorption systems are dominated by a single line,[43,44] the N 1s x-ray photoelectron spectroscopy (XPS) spectrum of N_2 on Ni(100) at $h\nu = 1486.6$ eV has been found to be composed of two peaks of nearly equal intensity.[49] Figure 16 shows our results recorded at $h\nu = 500$ eV, i.e., about 100 eV above the N 1s threshold. As compared to the XPS spectrum, the high BE peak labeled U in Fig. 16 is reduced relative to the low BE peak S. The two BE positions are also indicated in Fig. 15. The position of peak S falls close to the onset of peak A while there is no absorption structure at the energy corresponding to the BE of peak U.

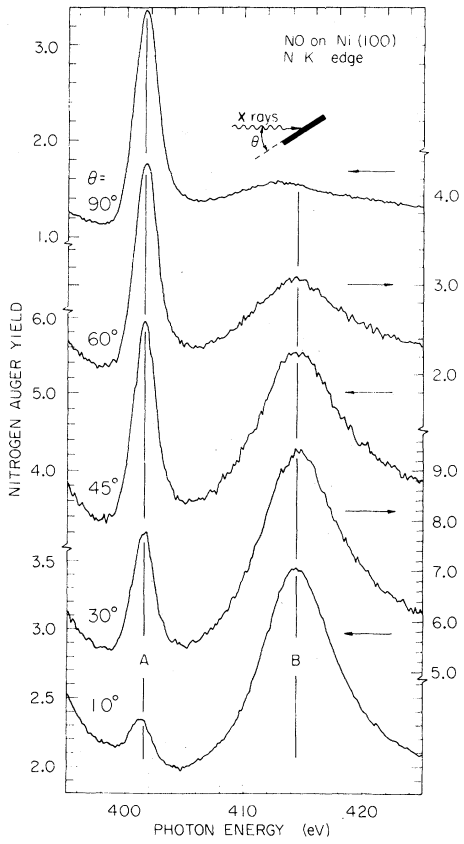

FIG. 13. NEXAFS spectra above the N K edge for NO on Ni(100) at $T=90$ K as a function of θ.

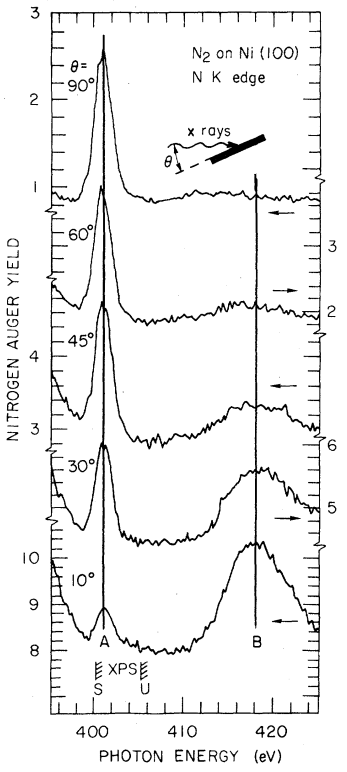

FIG. 15. NEXAFS spectra above the N K edge for N_2 on Ni(100) at $T=90$ K as function of θ. The binding energies of the N 1s core-line components are denoted by S (screened) and U (unscreened), respectively.

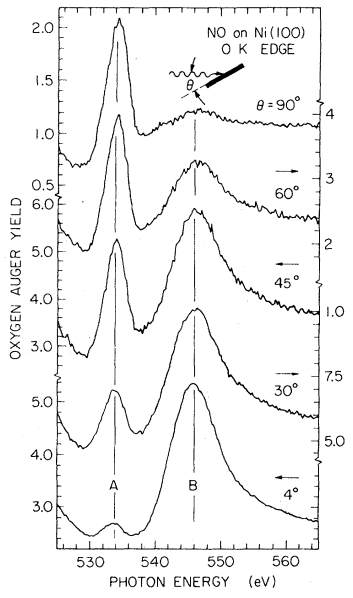

FIG. 14. Same as Fig. 13 above the O K edge.

IV. INTERPRETATION OF K-ABSORPTION-EDGE RESONANCES

A. Assignment of resonances

The assignment of the K-absorption-edge structures in Figs. 10–15 is greatly facilitated by the availability of gas-phase absorption,[1–6] electron energy-loss[8–11] data, and theoretical calculations.[12,13,50–55] Results for CO obtained by electron

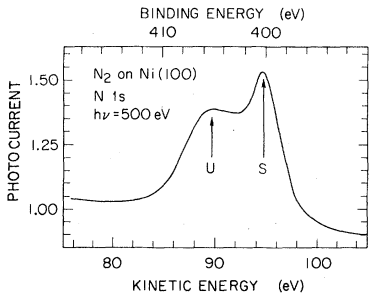

FIG. 16. Photoemission spectra of the N 1s core line for N_2 on Ni(100) at 90 K and $h\nu=500$ eV.

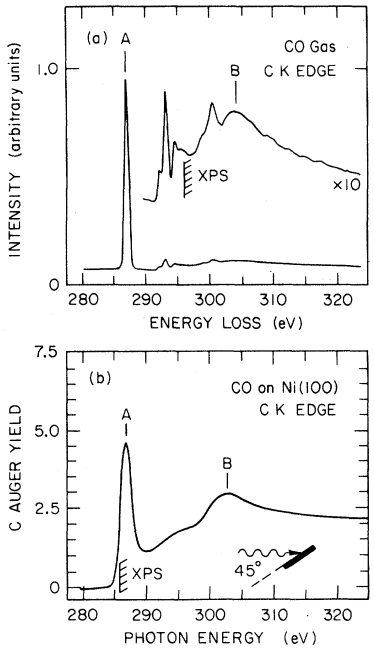

FIG. 17. Comparison of gas-phase (Ref.8) (a) and chemisorbed (b) absorption-edge fine structure near the C K edge for molecular CO. Photoemission binding energies (ionization potentials) are denoted by XPS.

energy-loss measurements[8] are shown in Fig. 17(a). For all studied molecules, *peak A* corresponds to a transition from a 1s initial state to a (at least partially) unoccupied molecular-orbital final state of π symmetry. This assignment was first made by Nakamura *et al.*[4] for N_2 gas and was confirmed by the calculations of Dehmer and Dill.[12,13] As shown for gas-phase CO on the left side of Fig. 18, a 1s (molecular notation 1σ or 2σ) electron is promoted into the empty 2π molecular orbital which for neutral CO lies above the vacuum level (E_V). In the absorption process, the 2π level is pulled below E_V by the Coulomb interaction with the created core hole resulting in an excitation energy ϵ_π, which is less than the 1s binding energy ϵ_B [see Table II and Fig. 18(a)]. The energy gained can be estimated[55] by the lowest ionization energy (i.e., of the 2π level) of the equivalent-core molecule. Since N_2^+ or C^+O with a 1s core hole are equivalent to NO, the Coulomb energy gained by placing an electron into the 2π orbital below the vacuum level should be approximately equal to the binding energy of the 2π level in NO. Table II shows that $\epsilon_\pi - \epsilon_B = 8.9$ eV for C^+O and N_2^+. This compares with the value 9.7 eV (Ref. 56) for the 2π binding energy in NO. Similarly, the difference $\epsilon_\pi - \epsilon_B = 10.8$ eV for N^+O is comparable to the lowest ionization potential 12.0 eV (Ref. 56) for O_2. The corresponding final state in absorption is a *bound state* where the excited electron remains on the molecule. The resonance excitation energies and the corresponding one-electron binding energies for gas-phase CO, NO, and N_2 are summarized in Table II.

In analogy to gas-phase spectra *peak B* in Figs.

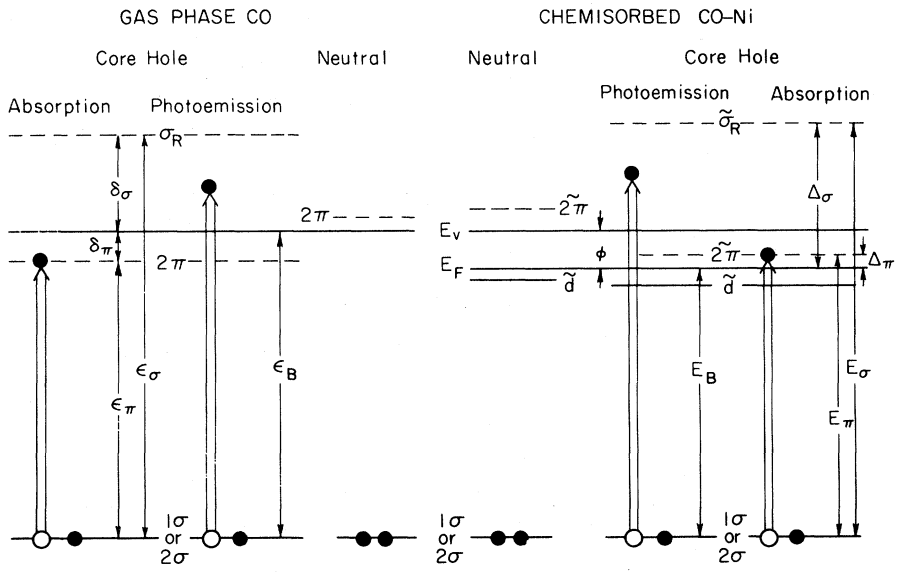

FIG. 18. Energy-level diagram for gas-phase and chemisorbed CO for the neutral (ground-state) and excited (core-molecule. E_B and ϵ_B are the one-electron binding energies measured in photoemission and E_π, ϵ_π, E_σ, and ϵ_σ the resonance positions measured in an absorption experiment.

TABLE II. Photoemission core binding energies and absorption resonance energies.

		Gas phase					Chemisorbed on Ni(100)				
Molecule	Hole state	ϵ_B[a] (eV)	ϵ_π[a] (eV)	ϵ_σ[a] (eV)	δ_π[a] (eV)	δ_σ[a] (eV)	E_B[a] (eV)	E_π[a] (eV)	E_σ[a] (eV)	Δ_π[a] (eV)	Δ_σ[a] (eV)
CO	2σ(C 1s)	−296.2[b]	287.3[e]	303.9[e]	−8.9	7.7	−285.8[g]	287.5	303.0	1.7	17.2
	1σ(O 1s)	−542.6[b]	534.1[e]	550.9[e]	−8.5	8.3	−531.6[g]	534.0	550.0	2.4	18.4
NO	2σ(N 1s)	−410.5[c]	399.7[f]	414.5[f]	−10.8	4.0	−399.9[h]	401.5	414.5	1.6	14.6
	1σ(O 1s)	−543.2[c]	532.7[f]	546.3[f]	−10.5	3.1	−530.6[h]	534.0	546.0	3.4	15.4
N_2	1σ(N 1s)	−409.9[d]	401.0[e]	418.9[e]	−8.9	9.0	−400.2[i] −405.3[i]	401.0	418.5	0.8[j]	18.3[j]

[a]See Fig. 18 for defintions.
[b]T. A. Carlson, M. O. Krause, and W. E. Moddeman, J. de Physique (Paris) 32, C4-76 (1971).
[c]D. P. Spears, H. J. Fischbeck, and T. A. Carlson, J. Electron Spectrosc. 6, 411 (1975); value is weighted average of two multisplit peaks.
[d]U. Gelius, J. Electron Spectrosc. 5, 985 (1974).
[e]A. P. Hitchcock and C. E. Brion, J. Electron Spectrosc. 18, 1 (1980).
[f]G. R. Wight and C. E. Brion, J. Electron Spectrosc. 4, 313 (1974).
[g]P. R. Norton, R. L. Tapping, and J. W. Goodale, Chem. Phys. Lett. 41, 247 (1976); C. R. Brundle (private communication) finds C 1s (285.6 eV) and O 1s (531.5 eV).
[h]Average of values for polycrystalline Ni: N 1s (399.9 eV) and O 1s (530.9 eV), C. R. Brundle, J. Vac. Sci. Technol. 13, 301 (1976), and for Ni(111): N 1s (400.0 eV) and O 1s (530.3 eV) M. J. Breitschafter, Diplomarbeit, T. U. München, 1980 (unpublished).
[i]J. C. Fuggle, E. Umbach, D. Menzel, K. Wandelt, and C. R. Brundle, Solid State Commun. 27, 65 (1978).
[j]Relative to the binding energy (400.2 eV) of the screened N 1s photoemission peak.

10—15 is assigned to a transition of a 1s electron to a resonance of σ symmetry in the continuum. At a particular excitation energy (ϵ_σ), the excited photoelectron can, owing to strong multiple scattering within the molecule, be trapped in quasibound resonant states in the continuum. In analogy to resonances observed in electron scattering by molecules,[57] this resonance is usually referred to as a "shape resonance."[13]

B. Chemisorbed versus gas-phase spectra

In the following discussion, we shall ignore the polarization dependence (see Secs. V and VI below) of the NEXAFS spectra in Figs. 10—15, but rather compare the general features and their energy positions to the gas-phase results. The gross features of the NEXAFS spectra closely resemble those for the corresponding gas-phase results for CO,[3,8,11,58,59] NO,[9] and N_2.[2,4,6,8,10,11] A comparison for CO is shown in Fig. 17. There are differences in the detailed fine structure between peaks *A* and *B* where the gas-phase spectra exhibit several sharp but weak resonances which correspond to transitions to Rydberg-type states just below the ionization energy. These Rydberg resonances appear to be completely smeared out in our spectra. Peak *A* is broader in our spectra than in the corresponding gas-phase spectra which we attribute mainly to a lower instrumental (monochromator) resolution.

The similarity of the chemisorbed and gas-phase spectra indicate that the former must be dominated by *intramolecular excitations* and that the molecule-substrate interaction has little influence on the *K*-edge resonance structures, apart from giving rise to the polarization dependence through alignment of the molecular axis relative to the surface. This is also corroborated by a comparison of the gas-phase resonance energies ϵ_π and ϵ_σ for peaks *A* and *B* with those labeled E_π and E_σ (Fig. 18) for the chemisorbed case. Table II shows that for CO and N_2 the difference between the respective π resonance positions ($E_\pi - \epsilon_\pi$) does not exceed 0.2 eV. For NO the shift is 1.3 eV for the O and 1.8 eV for the N edge. The shape resonance positions E_σ and ϵ_σ agree to better than 1 eV in all cases. The basic reason for the close correspondence of the resonance excitation energies for gas-phase and chemisorbed molecules lies in the fact that *initial-state binding energy shifts upon chemisorption are small and that the resonance energies are not modified by extramolecular relaxation* (i.e., screening of the core hole by charge transfer from the substrate) in con-

trast to the photoemission binding energies.

The conventional picture of chemisorption of the isoelectronic molecules CO (Ref. 24) and N_2 (Refs. 60–62) on *d*-band metals is charge transfer to the metal from the highest occupied σ molecular orbitals (5σ for CO and 4σ, 5σ for N_2) and charge back donation into the first unoccupied 2π molecular orbital. Of interest here is mainly the effect of chemisorption on the 2π orbital. The ground state of the adsorbate-substrate complex will involve mixing of the 2π molecular orbital with metal $d\pi$ and to some extent, $sp\pi$ (Refs. 30 and 62) orbitals. This results in the formation of a filled bonding $\tilde{d}\pi$ and an empty antibonding $2\tilde{\pi}$ orbital. For Ni, the *empty* $2\tilde{\pi}$ orbital (Fig. 18) formed upon chemisorption will have some Ni $3d\pi$ character. Peak *A* in Figs. 10–12 and 15 corresponds to transitions into this empty $2\tilde{\pi}$ state. The *filled* metal $3\tilde{d}\pi$ states, on the other hand, will contain some small[61–64] ($\sim 0.1e$) ligand 2π admixture. It is this filled state which for CO has been observed in photoemission studies of the valence-band region.[26]

Free NO differs from CO and N_2 in that the 2π state is singly occupied with an ionization potential of 9.7 eV.[57] Using a value of $\phi = 5.5$ eV for the work function, this would correspond to a 2π binding energy of 4.2 eV relative to the Fermi level for an *unperturbed* chemisorbed NO molecule. Because their binding energies are comparable, the NO 2π state will strongly hybridize with metal, $d\pi$ states. Again, an empty $2\tilde{\pi}$ and occupied $3\tilde{d}\pi$ orbital will be formed. For NO, the admixture of the pure ligand and metal states is stronger than for CO and the $3\tilde{d}\pi$ state will have significant 2π character ($\sim 1.0e$).[65] This latter state has been observed about 2 eV below the Fermi level in photoemission studies for the substrates Ni(111),[66] polycrystalline Ni,[65] Pt(100),[67] Ir(100) and Ir(111),[68] Pd(111),[69] and Ru(001).[70] As for CO and N_2, the absorption peak *A* for NO on Ni(100) in Figs. 13 and 14 corresponds to a transition from a 1*s* initial state to the $2\tilde{\pi}$ state above the Fermi level.

The difference $E_\pi - \epsilon_\pi$, which is within the 0.5-eV experimental error (energy calibration) for CO and N_2, and amounts to 1.5 ± 0.5 eV for NO, is mostly due to the shift of the ligand 2π state upon hybridization with the metal $d\pi$ states to form the empty antibonding $2\tilde{\pi}$ orbital. As the 2π and $d\pi$ orbitals hybridize, the $2\tilde{\pi}$ antibonding state is pushed up in energy from the 2π position while the $\tilde{d}$ bonding state is lowered relative to the pure $d\pi$ states. For CO and N_2, the empty ligand 2π state lies above the vacuum level, ~ 8 eV higher than the center of the Ni *d* band. Thus, upon hybridization, the admixture,[61] charge transfer, and shift are small. For NO, the singly occupied ligand 2π state lies about 4 eV below the Fermi level only about 2 eV from the center of the Ni *d* band. Thus, hybridization[62] and the shift are expected to be larger in agreement with our experimental observation.

C. Resonance energies and binding energies

What remains to be explained are the comparable π resonance energies for the gas-phase (ϵ_π) and the chemisorbed (E_π) molecules. Also, the π resonance energies are close to the photoemission 1*s* BE's (E_B) for the chemisorbed case but are about 5 eV smaller than the gas-phase 1*s* ionization potentials (ϵ_B) corrected for the work function.

In discussing resonance energies and comparing them to photoemission binding energies we need to remember that both are measured for an *excited state* (core hole) of the molecule-metal surface complex. In the previous discussion of the bonding we assumed a *neutral ground state* and ignored the presence of the core hole. As discussed above the ground-state properties will change upon chemisorption and will be reflected in absorption and photoemission spectra as chemical-shift effects. However, for the molecules discussed here these *initial-state* effects are small (0–2 eV). More important is the response of the local electronic configuration to the creation of the core hole. Such *final-state* effects play the most important role in understanding the position of the *K*-edge absorption resonances and its relationship to the 1*s* binding energies determined by photoemission.

The 1*s* BE in *photoemission* is referenced to the vacuum level E_V for the free molecule (ϵ_B) and the Fermi level E_F for the chemisorbed molecule (E_B). The so-determined BE's of the main 1*s* photoemission peaks for CO, NO, and N_2 differ by about 10 eV as seen from Table II. Correction for the different reference levels by using a work function of 5 eV leaves us with an ~ 5 eV lower 1*s* BE for the chemisorbed than for the free molecule. This energy difference has its main origin in the energy which can be gained by the *screening* of the 1*s* core hole through charge transfer from the metal. For the three molecules of interest the screening charge is transferred from the metal *p* or *d* electrons to the molecular 2π state. This charge transfer can be envisioned as the occupied bonding $\tilde{d}\pi$ state (see Sec. IV B) having more molecular 2π character in the presence of a core hole than for the ground-state case.[31,32] The metal-to-ligand charge transfer has

also been referred to as a "shake-down" process,[30] i.e., charge transfer from the Fermi level to the $d\tilde{\pi}$ orbital below E_F when the core hole is created.

The first resonance (A) in the K-edge absorption spectra corresponds to a bound-state transition. Here the excited $1s$ electron occupies the 2π or $2\tilde{\pi}$ orbital and effecitvely screens the $1s$ core hole. Thus no or little metal-to-ligand screening charge transfer takes place and the gas-phase and chemisorption $1s \rightarrow 2\pi$ resonance energies are comparable. Furthermore, the final state in absorption resembles the screened final state in photoemission since in both cases the $1s$ hole is screened by a charge in the molecular 2π orbital. This is why the peak A resonance energies for CO and NO fall close to the $1s$ photoemission BE's (labeled XPS in Figs. 6 and 7).

For chemisorbed CO and NO the $1s$ photoemission spectrum is dominated by a single core line with some weaker satellites at higher BE.[71] For N_2 on Ni(100) (Refs. 49, 71, and 72) and on several other substrates[71] two lines are observed which at XPS energies are of equal intensity. Even for excitation energies ($h\nu \approx 410$ eV) very close to threshold (~ 10 eV above E_F) the N $1s$ core spectrum consists of two lines of comparable intensity.[73] These lines are labeled U and S in the spectrum shown in Fig. 16. In contrast, the N_2 absorption spectrum resembles those of CO and NO and exhibits no satellite structure near peak A. As for CO and NO peak A falls close to the BE of the lowest BE $1s$ photoemission peak which is labeled S in Figs. 15 and 16.

The N $1s$ double-peak structure for N_2 on Ni(100) arises from final-state screening effects for weakly chemisorbed molecules. It was first explained by Fuggle *et al.*[49] using a model suggested[29,74] by Schönhammer and Gunnarsson. In this model the *screened* peak S is attributed to a $1s$ excitation where the core hole is screened by metal-to-ligand charge transfer (shake-down) as discussed above.[30–32] The *unscreened* peak U results from a shake-up transition[31] from the occupied $d\tilde{\pi}$ to the empty $2\tilde{\pi}$ orbital. The final state is called "unscreened" because the shake-up transition corresponds to a charge transfer from the adsorbate to the substrate. As suggested by Umbach[71] this picture is consistent with the various theoretical models discussed in the literature.[30–32] The final state in absorption is very similar to the screened photoemission final state except that the screening charge is provided by the excited bound-state electron rather than charge transfer from the metal. Therefore, after the $1s \rightarrow 2\tilde{\pi}$ excitation the $2\tilde{\pi}$ state has little metal $d\pi$ admixture and is located predominantly on the molecule. The $d\tilde{\pi}$ state has little ligand 2π admixture similar to the ground-state case. Thus the lowest photoemission final state ($1s$ core hole, metal to 2π screening charge transfer) differs from that in absorption ($1s$ core hole, 2π bound state as screening charge) in that the bonding $d\tilde{\pi}$ state has only little charge density on the molecule. Therefore, the $d\tilde{\pi} \rightarrow 2\tilde{\pi}$ shake-up has almost zero probability for the K absorption process in the molecule and no corresponding shake-up or unscreened state is observed.

D. Resonance positions and molecular bond lengths

Blyholder[24] first suggested that the metal $d\pi$ to adsorbate 2π charge transfer ("back bonding") results in a strengthening of the metal-adsorbate bond but *weakens* the intramolecular bond. This is intuitively clear since the 2π orbital is antibonding in nature. The softening of the intramolecular bond on chemisorption is usually held responsible for an enhancement of the infrared absorption intensity of the molecular stretching mode[24,75] and for a reduced vibrational frequency, although this view has recently been challenged.[76]

From a structure point of view the intramolecular bond length R for a chemisorbed molecule should be longer than for the free molecule ($R_{NO} = 1.151$ Å, $R_{CO} = 1.130$ Å, and $R_{N_2} = 1.094$ Å).[77] It has recently been pointed out by Bianconi *et al.*[33] that the energy position of final-state shape resonances is directly sensitive to the intramolecular bond length. This is anticipated from a simple EXAFS-like picture where the scattering of the photoelectron wave by the neighbor atom leads to a final-state interference effect. Since the scattering is in momentum space an inverse relationship results between bond length and the separation of the scattering maxima or the separation of a given scattering maximum from threshold. Qualitatively this explains the separation $\Delta\epsilon_{\pi\sigma}$ of the π and σ resonance positions for the free molecules as summarized in Table III. $\Delta\epsilon_{\pi\sigma}$ is largest for N_2, the molecule with the shortest R and the least for NO which has the longest internuclear distance. The best calibration of bond length changes with resonance energy shifts is obtained by comparison of the $\Delta\epsilon_{\pi\sigma}$ and R values for the isoelectronic free molecules CO and N_2. We obtain $\Delta R = 0.03$ Å for a resonance shift of 1 eV. This value is close to that calculated (0.04 Å/eV) for the change in the C-N distance in

$Fe(CN)_6$ as a function of the shape resonance positions above the Fe K edge.[33]

Quantitative analysis of the resonance shifts upon chemisorption for CO, NO, and N_2 is impeded by the presence of initial-state shifts as discussed earlier. These effects are large ($\sim 1-2$ eV) when the energy separations of the π and σ resonances are compared since the 2π level is involved in the chemisorption bond. Initial-state effects are minimized by directly comparing the gas-phase (ϵ_σ) and chemisorption (E_σ) shape resonance positions. As listed in Tables II and III the σ resonance is always shifted to *lower* energy upon chemisorption by $0-1$ eV indicating an *increase* of the intramolecular bond length of the order of 0.03 Å or less.

TABLE III. Separation of gas-phase and chemisorption resonances.

Molecule	Hole state	Gas phase $\Delta\epsilon_{\pi\sigma}$[a] (eV)	Chemisorption $\Delta E_{\pi\sigma}$[a] (eV)	Δ[b]	$\epsilon_\sigma - E_\sigma$
CO	2σ(C 1s)	16.6	15.5	1.1	0.9
	1σ(O 1s)	16.8	16.0	0.8	0.9
NO	2σ(N 1s)	14.8	13.0	1.8	0
	2σ(O 1s)	13.6	12.0	1.6	0.3
N_2	1σ(N 1s)	17.9	17.5	0.4	0.4

[a]Separation between π and σ resonances.
[b]$\Delta = \Delta\epsilon_{\pi\sigma} - \Delta E_{\pi\sigma}$.

V. THEORETICAL ASPECTS OF POLARIZATION-DEPENDENT PHOTOEMISSION AND ABSORPTION

A. Photoemission

In deriving an expression for the polarization dependence of molecular-resonance peak intensities at *absorption* thresholds let us start from the more general equation which governs the peak intensities in polarization-dependent angle-resolved *photoemission* spectroscopy (PARPES) of oriented molecules. We will assume throughout this section that the symmetry of the molecular orbitals is not destroyed on adsorption, that the molecule possesses an axis $\vec{M}$ of cylindrical symmetry and that the exciting photon radiation is linearly polarized. With the angular definitions of Fig. 19 the one-electron cross section for photoemission along the direction $\vec{k}$ can then be expressed in closed form[78]

$$\frac{d^2\sigma}{d\vec{k}d\vec{M}} = I(\epsilon,\phi,\delta) = A(\epsilon)\cos^2\delta + [B(\epsilon)+C(\epsilon)\cos 2\phi]\sin^2\delta + D(\epsilon)\sin\phi\sin\delta\cos\delta \,. \quad (1)$$

Here δ is the angle between the molecular axis $\vec{M}$ and the $\vec{E}$ vector and the photoemission direction $\vec{k}$ is specified by the polar coordinates ϵ and ϕ. Both the Poynting and $\vec{E}$ vectors are chosen to be in the (y,z) plane of the molecular frame. The functions $A(\epsilon)$, $B(\epsilon)$, $C(\epsilon)$, and $D(\epsilon)$ can be calculated for a particular photon energy from first principles.[78] In PARPES one measures molecular valence- or core-level intensities as a function of the *photon energy* ($h\nu$) and the *photon-polarization direction* ($\vec{E}$) and *electron-emission direction* ($\vec{k}$) relative to the substrate. Several approaches are possible to determine the molecular orientation relative to the substrate.

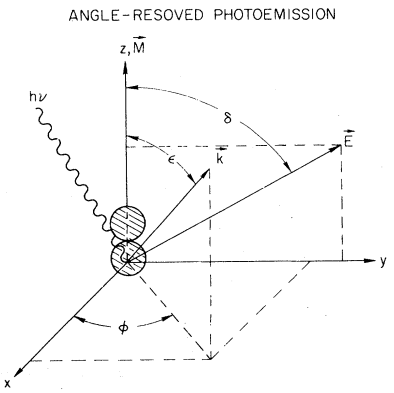

FIG. 19. Definition of the coordinates which determine the polarization-dependent angle-resolved photoemission spectra from oriented molecules. $\vec{M}$ is the symmetry axis of the molecule, $\vec{E}$ the x-ray electric field vector, and $\vec{k}$ the photoelectron emission direction.

At a given photon energy $\vec{E}$- and $\vec{k}$-dependent intensity distributions can be compared to those calculated from Eq. (1).[79–82] For the correctly assumed adsorbate-substrate orientation the measured and calculated intensity distributions should match. Often the application of mirror-plane symmetry rules[83,84] greatly facilitates the derivation of the molecular orientation. If the detector lies in a mirror plane only even-parity initial states can be detected with $\vec{E}$ in the mirror plane and only odd-parity states for $\vec{E}$ perpendicular to the mirror plane. With the use of such symmetry rules it can be shown[78] that $B(\epsilon) = -C(\epsilon)$ for σ initial states

and $A(\epsilon)=0$ for π states. Also for $\epsilon=0$, $C(0)=D(0)=0$.

The most powerful method to determine the molecular orientation uses the fact that for many molecules final-state shape resonances of pure symmetry can be observed. It is important to point out that such resonances lie in the continuum and are thus superimposed on a background due to nonresonant excitation channels of π final-state symmetry which might also exhibit a weak energy dependence.[13,54] In addition, the shape resonance might interfere with structure due to multielectron excitation processes[8-11] which would still be present even though the shape resonance was absent.[85] For σ initial states (e.g., 4σ or 1σ) the shape-resonance photoemission intensity exhibits a sharp maximum for $\vec{E}||\vec{k}||\vec{M}$. We can use this concept two ways. First for $\vec{k}||\vec{M}$ ($\epsilon=0$) and σ initial states [$B(0)=C(0)=D(0)=0$] Eq. (1) reduces to

$$I(\epsilon=0,\delta)=A(0)\cos^2\delta \ . \tag{2}$$

Thus if we map out the polarization dependence (δ) of the shape-resonance intensity by keeping the relative detector-sample orientation fixed ($\vec{k}||\vec{M}$) we should be able to make the resonance vanish for $\delta=90°$ or $\vec{E}\perp\vec{M}$. Secondly, if we choose $\vec{E}||\vec{M}$ ($\delta=0$) we obtain

$$I(\epsilon,\delta=0)=A(\epsilon) \ . \tag{3}$$

Since $A(\epsilon)$ peaks for $\epsilon=0$ ($\vec{k}||\vec{M}$) we should obtain the maximum shape resonance intensity when the detector acceptance lies along the molecular axis. These concepts have been successfully employed to determine the orientation of CO on Ni(100) (Refs. 15 and 17), and Ni(111) (Ref. 18) and CO on Cu(100).[16]

B. Absorption

In an x-ray absorption experiment the absorption coefficient (μ) of the molecule at and above a core-electron excitation threshold is being measured. The absorption coefficient of a particular inner shell is by definition the cross section for a photoexcitation of an electron from that shell. It thus includes bound-state as well as continuum-excitation (ionization) probabilities. In a photoemission experiment bound-state transitions are of course not observable since the excited electron never leaves the molecule but they are formally included in the cross-section equation (1). Thus the absorption coefficient can simply be obtained by integrating Eq. (1) over all electron emission angles $\vec{k}$. Because of cylindrical symmetry the last two terms in Eq. (1) vanish and we obtain

$$\mu(\delta)=\frac{d\sigma}{d\vec{M}}=X\cos^2\delta+Y\sin^2\delta \ . \tag{4}$$

The coefficients X and Y in Eq. (4) can be evaluated as[86]

$$X=\frac{\sigma}{4\pi}(1+\beta_m) \tag{5}$$

and

$$Y=\frac{\sigma}{4\pi}(1-\tfrac{1}{2}\beta_m) \ ,$$

such that Eq. (2) assumes the simple form[86]

$$\mu(\delta)=\frac{\mu_0}{4\pi}[1+\tfrac{1}{2}\beta_m(3\cos^2\delta-1)] \ . \tag{6}$$

Here μ_0 is the integrated photoabsorption cross section (random molecular orientation) and $\beta_m=\beta_m(h\nu)$ is an asymmetry parameter. For s (σ) initial states β_m can be expressed in terms of the electric dipole transition amplitudes $D^2_{\sigma\sigma}$ for $\sigma\rightarrow\sigma$ and $D^2_{\sigma\pi}$ for $\sigma\rightarrow\pi$ transitions[86,87] as follows:

$$\beta_m(h\nu)=\frac{2[D^2_{\sigma\sigma}(h\nu)-D^2_{\sigma\pi}(h\nu)]}{[D^2_{\sigma\sigma}(h\nu)+2D^2_{\sigma\pi}(h\nu)]} \ . \tag{7}$$

Note that because of the above form of β_m the photoabsorption cross section $\mu(\delta)$ contains no interference terms between σ and π ionization amplitudes. Thus for pure σ and π final states we obtain $\beta_m=2$ and $\beta_m=-1$, respectively, and Eq. (6) assumes the simple forms

$$\mu_{\sigma\sigma}(\delta)=\frac{3\mu_0}{4\pi}\cos^2\delta \tag{8}$$

and

$$\mu_{\sigma\pi}(\delta)=\frac{3\mu_0}{8\pi}\sin^2\delta \ . \tag{9}$$

Equations (8) and (9) express the intuitive intensity distributions for different orientation of the $\vec{E}$ vector with respect to the molecular axis. In the dipole approximation s electrons are excited along the electric field vector direction. For $\vec{E}||\vec{M}$ ($\delta=0$) the excited electron wave function must therefore have σ symmetry ($\mu_{\sigma\pi}=0$) while for $\vec{E}\perp\vec{M}$ ($\delta=90°$) the final state must be of π symmetry ($\mu_{\sigma\sigma}=0$).

For chemisorption systems the molecular symmetry axis may be inclined by an angle α from the surface normal of the substrate as shown in Fig. 20. Absorption spectra are measured for different an-

gles of grazing incidence θ with the $\vec{E}$ vector typically lying in the plane of incidence. The polarization dependence of the molecular absorption coefficient in the frame of the molecule is given by Eq. (6). Here we have assumed that the orientation of the electric field vector at the surface is unchanged from that of the incident x rays. In the soft x-ray region ($h\nu > 280$ eV) this is true within the angular uncertainties of the measurements. In order to obtain the corresponding expression in the reference frame (x',y',z') of the sample (Fig. 20) we can express $\cos^2\delta$ in terms of trigonometric functions involving the angles α, θ, and ϕ. Depending on the symmetry of the substrate, its domain orientations, and the molecular bonding configuration, the bent molecule will in general occupy several azimuthally equivalent positions. It can be shown in general that for *higher than twofold* orientational symmetry the absorption coefficient does no longer depend on the details of the azimuthal (ϕ) molecular orientation. Apart from an overall normalization constant it is then equivalent to assume cylindrical symmetry about the sample normal. This describes almost all cases of practical interest. If in addition we allow

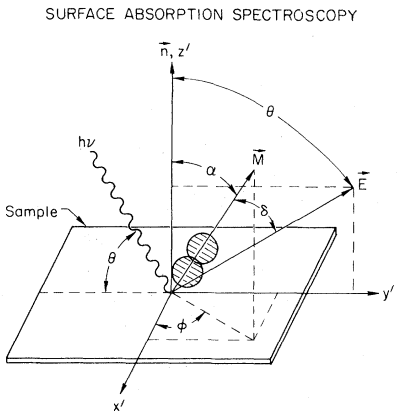

FIG. 20. Coordinates which describe the polarization-dependent absorption spectra for chemisorbed molecules. $\vec{n}$ is the surface normal, $\vec{M}$ the molecular symmetry axis, and $\vec{E}$ the electric field vector.

for an uncertainty in the polar tilt angle $0 \le \alpha_1 \le \alpha \le \alpha_2$ (e.g., due to vibrational bending), we can obtain the polarization-dependent absorption coefficient $\mu(\alpha_1,\alpha_2,\theta)$ for the tilted molecule by integration,

$$\mu(\alpha_1,\alpha_2,\theta) = \int_0^{2\pi}\int_{\alpha_1}^{\alpha_2} \mu(\alpha,\theta,\phi)\sin\theta\, d\theta\, d\phi \Big/ \int_0^{2\pi}\int_{\alpha_1}^{\alpha_2} \sin\theta\, d\theta\, d\phi \ , \tag{10}$$

or

$$\mu(\alpha_1,\alpha_2,\theta) = \mu_0\{1+\tfrac{1}{4}\beta_m(3\cos^2\theta-1)[(\cos^3\alpha_1-\cos^3\alpha_2)/(\cos\alpha_1-\cos\alpha_2)-1]\} \ . \tag{11}$$

Equation (11) describes the polarization dependence (θ) of any absorption peak which corresponds to a transition of a s (σ) initial state to a final state of mixed $-1 < \beta_m < 2$ or pure π ($\beta_m = -1$) and/or σ ($\beta_m = 2$) symmetry for a molecule which is tilted by an angle $\alpha_1 \le \alpha \le \alpha_2$ from the surface normal. In practice one measures the polarization dependence of absorption-threshold peaks which correspond to either a strong transition to a discrete (bound) final state of pure symmetry or to a transition to a resonant final state in the continuum (shape resonance). The experimental intensities are then fitted to Eq. (11) by leaving the tilt angle α as the only adjustable parameter.

VI. EXPERIMENTAL DETERMINATION OF MOLECULAR ORIENTATION

A. Normalization of measured peak intensities

Quantitative comparison of the polarization dependence of experimental-resonance peak intensities with theory requires careful normalization of the measured peak areas. The task is to *eliminate all geometry effects which arise from rotating the sample relative to the detector.* Apart from intrinsic polarization-dependent effects geometry-induced changes of the total adsorbate Auger signal arise from changes in the sampled number of adsorbing molecules and from diffraction[88–90] and escape-depth effects. Thus the peak areas need to be normalized by a signal from the molecule which is intrinsically isotropic with respect to polarization changes but is modified by geometry effects similar to the resonance peak intensities. The problem is identical to that in polarization-dependent surface EXAFS (SEXAFS) studies where the measured intensity oscillations above the edge need to be normalized to a single absorbing atom and nonpolarization-dependent geometry effects.[91,92] In EXAFS and SEXAFS this is accomplished by using the isotropic atomic absorption as a reference which is reflected by the overall jump at the absorption edge. Because of the presence of dominating resonances it is difficult to define the edge jump in

NEXAFS. One therefore has to monitor the isotropic continuum molecular K-shell absorption as a reference. Since the diffraction of the (constant energy) Auger electrons is photon-energy independent the Auger intensity for a photon energy considerably above the K threshold (~ 100 eV) can be used for this purpose. Our measurements showed that even with the partially angle integrating CMA geometry effects between normal and grazing angles of incidence can be as large as a factor of 2.

Another way to account for geometry effects is to use a model system. This model with well-known molecular orientation on the same substrate can then be used for comparison with the system under investigation. Both data acquisition and analysis should be done in an identical fashion.

B. Effect of incomplete x-ray polarization

At present, the incomplete polarization of the monochromatized synchrotron radiation is one of the factors which limit the accuracy of the determination of molecular orientation. The incident x rays are elliptically polarized with an intensity component $I_{||}$ polarized in the horizontal plane of the electron orbit and a vertical component $I_{\perp}$ ($\ll I_{||}$). In the synchroton radiation literature, the degree of linear polarization in the plane of orbit is usually defined as [93]

$$P = I_{||}/(I_{||}+I_{\perp}) . \tag{12}$$

In the soft x-ray region, the radiation from the storage ring integrated over typical vertical monochromator acceptance angles is about 75–80 % polarized.[93] P is enhanced by vertical grazing incidence reflections of the x rays by the optical elements of the beam line.

For the grasshopper monochromator at SSRL, we can estimate the polarization of the beam incident on the sample from the angular variation of the measured peak A intensities for CO on Ni(100) (Figs. 10 and 11). Since it has been well established that the CO molecular axis $\vec{M}$ is accurately aligned along the surface normal changes in the resonance A intensity with θ arise from the variation of the electric field vector component $\vec{E}_{||}$ (see Fig. 21). The component $\vec{E}_{\perp}$ remains constant for all θ. Thus, for normal incidence ($\theta = 90°$) both $\vec{E}_{||}$ and $\vec{E}_{\perp}$ are perpendicular to $\vec{M}$ and can thus excite the π resonance (peak A). In this case, the peak A intensity is proportional to $(\vec{E}_{||})^2+(\vec{E}_{\perp})^2$ or $I_{||}+I_{\perp}$. For grazing incidence, only $\vec{E}_{\perp}$ can excite the π resonance and the residual peak-A intensity is a measure of $(\vec{E}_{\perp})^2$ or $I_{\perp}$. For CO on Ni(100), we obtain from Fig. 21 and including a correction for geometry effects (Sec. VI A) the values $I_{||}+I_{\perp}=4.10\pm0.05$ and $I_{\perp}=0.58\pm0.11$. This yields $P=0.86\pm0.05$. We note that this method appears to be quite useful for the determination of the x-ray polarization in the soft x-ray region.

The finite vertical polarization component leads to problems when the measured θ dependence of the peak-A intensities is compared to theory [Eq. (11)]. The residual peak intensity at low θ values (Fig. 21) mimics a tilted molecular orientation. Hence, a fit of the uncorrected data points in Fig. 21 by means of Eq. (11) yields a tilt angle $\alpha = 14°$ (Fig. 20) as shown by the dashed curve in Fig. 21. It is, therefore, important to assess the effects of incomplete polarization by studying a model system and then apply the same correction procedure to the model and the unkown as discussed below.

C. Analysis of bound-state (π) resonance intensities

Determination of the area under the π bound-state transition (peak A) is straightforward in all studied cases. Because of its energy position it is not modified by any underlying absorption structure resulting from one- or multielectron transitions to continuum states. Therefore, the extraction of the π resonance-intensity changes with incidence angle is less problematic than for the shape resonance.

For the determination of the molecular orientation the peak-A areas were determined for several experimental runs and normalized to the incident

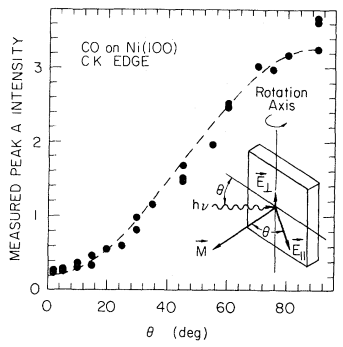

FIG. 21. Uncorrected measured peak-A resonance intensities for CO on Ni(100). Orientation of the components $\vec{E}_{\perp}$ and $\vec{E}_{||}$ of the elliptically polarized synchrotron radiation relative to the sample are also shown.

photon flux and to the background intensity at the peak-A position. At the time of the measurements we did not record the Auger intensity at an excitation energy far above threshold. Therefore, the peak-A intensities were not corrected for the geometry effects discussed in Sec. VI A. Instead we used the CO on Ni(100) system as our standard and corrected all measured peak-A intensitites for CO, NO, and N_2 in an identical fashion. At first, all intensities were normalized with respect to each other at the "magic angle" $\theta=54.7°$. It can be shown from Eq. (11) that at this angle the peak-A intensity is independent of the molecular orientation. Second, the same small correction was subtracted from all measured peak-A intensities to account for effects due to incomplete polarization.

The so-obtained peak-A intensities for CO and NO are compared in Fig. 22 to the angular dependence calculated from Eq. (11) as a function of a molecular tilt angle α from the surface normal. Because of the fourfold substrate symmetry we assumed a cylindrically symmetric tilt around the normal within limits $\alpha_1=\alpha-1°$ and $\alpha_2=\alpha+1°$. For the case $\alpha=0$ Eq. (11) was evaluated for $\alpha=\alpha_1=0$ and $\alpha_2=1°$ since per definition $\alpha_1\geq 0$. The 2° angular spread to some degree accounts for vibrational motion of the molecule.[94] In both cases best agreement between experiment and the calculation is obtained for $\alpha=0°$, i.e., alignment of the molecule along the surface normal. For a molecule lying down, the angular intensity dependence should be reversed from that observed. For a 54.7° tilt no polarization dependence should be observable. When CO is used as a reference, the comparison between the measured and calculated peak-A intensity changes implies that the molecular axis for NO at saturation coverage is oriented along the normal with an experimental uncertainty of $\pm 10°$. For N_2 the angular dependence of the peak-A intensity and, therefore, the molecular orientation is similar to CO and NO. In all cases the peak-A intensity changes by a factor of >10 between normal and grazing x-ray incidence.

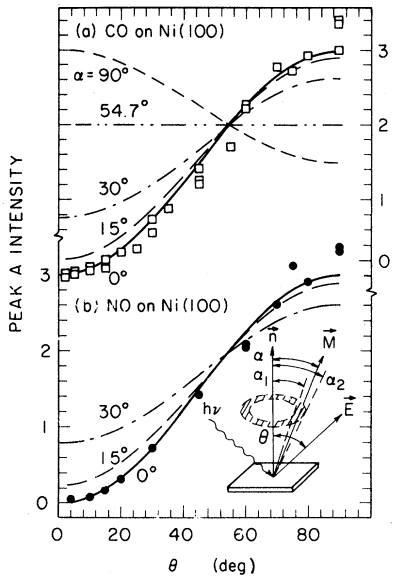

FIG. 22. (a) Corrected experimental peak-A intensity for CO on Ni(100) as a function of θ (squares). Lines are calculated intensity variations with θ [Eq. (11)] as a function of molecular tilt angle $\alpha_1=\alpha-1°$ and $\alpha_2=\alpha+1°$ as shown in the inset. (b) Same as in (a) for NO on Ni(100) (circles).

D. Analysis of shape-resonance (σ) intensities

Because the σ shape resonance falls into the continuum it is superimposed onto other one-electron ionization channels of π symmetry and other final-state channels involving multielectron excitations. This is illustrated in Figs. 23–25 for the C K edge of CO and the N K edge of NO and N_2 on N(100). In the upper half (a) we compare the structure of the peak-B region for the two extreme incidence angles $\theta=10°$ and 90°. In all cases the spectra exhibit a broad and weak residual peak Y for $\theta=90°$, i.e., in the case where $1s\rightarrow\sigma$ excitations are symmetry forbidden for a molecule aligned along the surface normal. The structure Y is centered at energies 296.5 eV (CO), 413 eV (NO), and 414 eV (N_2) and is lower than peak B by ~7 eV for CO, ~2 eV for NO, and ~4 eV for N_2. Care must be exercised that such

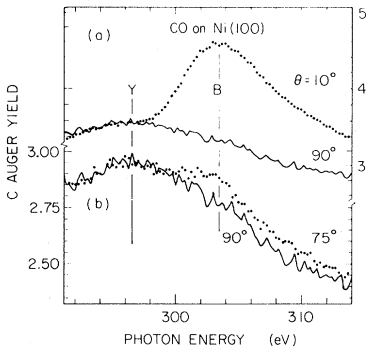

FIG. 23. Polarization dependence of the NEXAFS spectra near the σ shape resonance above the C K edge for CO on Ni(100). Note that the shape resonance (B) vanishes for $\theta=90°$.

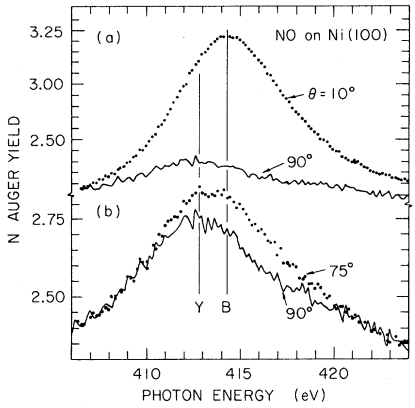

FIG. 24. Same as Fig. 23 for the N K edge of NO on Ni(100).

structures in the continuum are not mistaken for a residual shape-resonance intensity. In fact, we believe that this identification erroneously occurred in the interpretation of angle-resolved photoemission spectra of NO on Ni(100) (Ref. 95) which lead to conclusion of a tilted molecular orientation. Figures 23—25(b) show that in the three cases studied the shape resonance B does indeed vanish for $\theta \rightarrow 90°$. This is further evidence for an upright orientation of all three studied molecules on Ni(100).

There is another possible explanation of the structures Y in Figs. 23—25. Rather than being due to continuum ionization channels they may be the result of the constant final-state measurement technique. As illustrated in Fig. 5 the Ni VB sweeps through the Auger window about 20 eV before the onset of the O K edge (peak A). For chemisorbed CO, NO, or N_2 the molecular 1π, 5σ, 4σ, and 3σ valence orbitals fall into the binding-energy region 5—35 eV. From Fig. 5 it can be seen that any valence orbital with a BE greater than 20 eV causes a structure which would underlie the absorption-edge features. Figure 26 shows the strength and binding energy of the molecular 3σ orbital at $h\nu = 270$ eV. For all three molecules the 3σ BE is seen to be about 29 eV. Thus for a Auger window setting of 263 eV for C and 379 eV for N and assuming a work function of 5 eV the 3σ orbital will sweep through the window at 297 and 413 eV, respectively. Peak Y falls almost exactly at these energies.

E. The orientation of CO, NO, and N_2 on Ni(100)

Our finding of upright orientation of CO on Ni(100) is in good accord with previous experimental results involving valence-[15,17,80—82] and core-level[18] PARPES studies, high-energy photoelectron diffraction measurements,[90] and LEED intensity measurements and analysis.[96,97] Previous PARPES studies[95] for NO on Ni(100) were inconclusive or supportive of tilted molecular orientation. Howev-

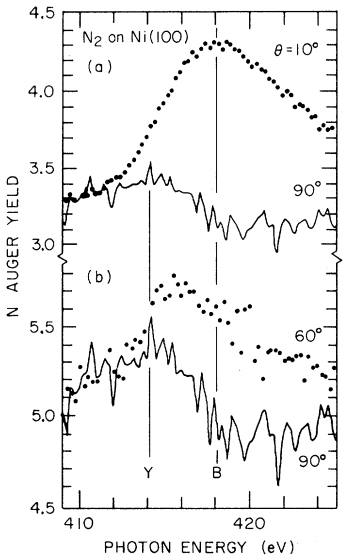

FIG. 25. Same as Fig. 23 for the N K edge of N_2 on Ni(100).

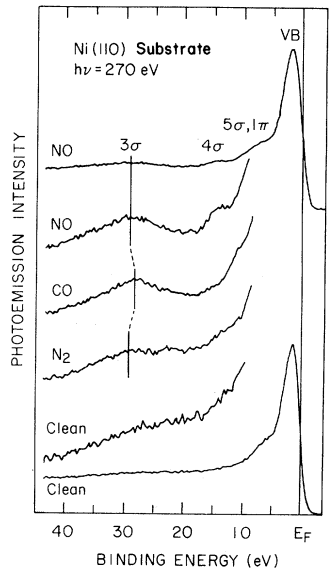

FIG. 26. Photoemission spectra at $h\nu = 270$ eV of the valence-band region for NO, CO, N_2 on Ni(110) ($T = 90$ K) and clean Ni(110).

er, our results for NO chemisorption at saturation coverage are in agreement with electron energy-loss studies for NO on Ni(111).[98] Note that NO has been suggested to be tilted on other surfaces[67,68,99] such that our results were not predictable *per se*. Previous photoemission studies[72] for N_2 on Ni(100) favored an upright orientation, and this is confirmed by our measurements.

VII. CONCLUSIONS

The present paper discusses core-electron absorption-edge spectra of chemisorbed molecules. Details of the experimental procedures are presented as well as results for three diatomic molecules chemisorbed on Ni(100). A discussion is given of the wealth of information contained in such spectra.

The NEXAFS spectra are shown to be dominated by intramolecular resonances. The gross features of the spectra are similar to those observed for the free molecules. Thus the spectra directly serve as a "fingerprint" of molecular versus atomic (dissociative) chemisorption. Deviations of the detailed resonance positions from the gas phase are discussed in terms of charge transfer of metal d valence electrons into the 2π molecular orbital upon chemisorption. This charge transfer affects the resonance positions through initial-state effects (chemical shifts) as well as final-state effects (resonance scattering in a stretched molecule).

Alignment of the molecular axis by the chemisorption bond leads to a strong polarization dependence of the NEXAFS spectra. The theory of this dependence is discussed in comparison with polarization-dependent angle-resolved photoemission and an analytical expression is derived which describes the observed resonance intensity variations. The orientation of CO, NO, N_2 on Ni(100) at saturation coverage is determined to be along the surface normal in all three cases.

With the availability of soft x-ray synchrotron radiation in the region of the C, N, and O K edges NEXAFS appears to be a new powerful surface technique. It can be used as a fingerprinting *technique* to determine what chemical species are present on the surface. In this respect it compliments low-energy electron-energy-loss spectroscopy. Furthermore, for chemisorbed molecules NEXAFS allows accurate determination of the molecular orientation on the surface. The sensitivity to the molecular alignment is as good as that of the most precise published PARPES measurements.[15–18] In comparison to PARPES the NEXAFS technique offers significant simplifications in data acquisition and interpretation since it depends solely on the $\vec{E}$ vector orientation relative to the sample. Finally, as will be reported elsewhere, NEXAFS can also be employed for structural studies of chemisorbed *atoms* since in this case the resonance scattering of the photoelectron is sensitive to the coordination of the atom on the surface. In fact, strong polarization-dependent effects have been observed[100] for O on Ni(100) which when compared to multiple scattering calculations[101,102] uniquely determine the chemisorption site.

ACKNOWLEDGMENTS

We would like to thank K. Baberschke, R. Treichler, and T. Kendelewicz for experimental help and J. W. Davenport, D. Dill, I. P. Batra, P. S. Bagus, and R. C. Brundle for valuable discussions. We would like to acknowledge J. E. Rowe for suggesting the acronym "NEXAFS". The work at SSRL was supported by the National Science Foundation under Contract No. DMR77-27489 in cooperation with the Stanford Linear Accelerator Center and the Basic Energy Division of the Department of Energy.

[1]M. J.-A. Prins, Physica 1, 1174 (1934); T. Magnusson, Nova Acta Regiae Soc. Sci. Ups. Ser. III, 11, 3 (1938).

[2]A. S. Vinogradov, B. Shlarbaum, and T. M. Zimkina, Opt. Spectrosc. 36, 383 (1974); 36, 658 (1974).

[3]D. M. Barrus, R. L. Blake, A. J. Burek, and K. C. Chambers, Phys. Rev. A 20, 1045 (1979).

[4]M. Nakamura, M. Sasanuma, S. Sato, M. Watanabe, H. Yamashita, Y. Iguchi, A. Ejiri, S. Nakai, S. Yamaguchi, T. Sagawa, Y. Nakai, and T. Oshio, Phys. Rev. 178, 80 (1969).

[5]W. Eberhardt, R. P. Haelbich, M. Iwan, E. E. Koch, and C. Kunz, Chem. Phys. Lett. 40, 180 (1976).

[6]A. Bianconi, H. Peterson, F. C. Brown, and R. Z. Bachrach, Phys. Rev. A 17, 1907 (1978); Chem. Phys. Lett. 58, 263 (1978).

[7]For a review, see F. C. Brown, in *Synchrotron Radiation Research*, edited by S. Doniach and H. Winick (Plenum, New York, 1980), p. 61.

[8]G. R. Wight, C. E. Brion, and M. J. van der Wiel, J. Electron Spectrosc. 1, 457 (1972/3).

[9]G. R. Wight and C. E. Brion, J. Electron Spectrosc. 4, 313 (1974).

[10]G. C. King, F. H. Read, and M. Tronc, Chem. Phys. Lett. 52, 50 (1977).

[11]A. P. Hitchcock and C. E. Brion, J. Electron Spectrosc. 18, 1 (1980).

[12]J. L. Dehmer and D. Dill, Phys. Rev. Lett. 35, 213 (1975).
[13]J. L. Dehmer and D. Dill, J. Chem. Phys. 65, 5327 (1976).
[14]E. W. Plummer, T. Gustafsson, W. Gudat, and D. E. Eastman, Phys. Rev. A 15, 2339 (1977).
[15]C. L. Allyn, T. Gustafsson, and E. W. Plummer, Chem. Phys. Lett. 47, 127 (1977).
[16]C. L. Allyn, T. Gustafsson, and E. W. Plummer, Solid State Commun. 24, 531 (1977).
[17]C. L. Allyn, T. Gustafsson, and E. W. Plummer, Solid State Commun. 28, 85 (1978).
[18]R. F. Davis, S. D. Kevan, D. H. Rosenblatt, M. G. Mason, J. G. Tobin, and D. A. Shirley, Phys. Rev. Lett. 45, 1877 (1980).
[19]J. Stöhr, K. Baberschke, R. Jaeger, R. Treichler, and S. Brennan, Phys. Rev. Lett. 47, 381 (1981).
[20]P. A. Lee, Phys. Rev. B 13, 5261 (1976).
[21]U. Landman and D. L. Adams, Proc. Nat. Acad. Sci. U. S. A. 73, 2550 (1976).
[22]P. H. Citrin, P. Eisenberger, and R. C. Hewitt, Phys. Rev. Lett. 41, 309 (1978).
[23]J. Stöhr, L. I. Johansson, I. Lindau, and P. Pianetta, Phys. Rev. B 20, 664 (1979)
[24]G. Blyholder, J. Phys. Chem. 68, 2772 (1964); J. Vac. Sci. Technol. 11, 865 (1974).
[25]E. W. Plummer, W. R. Salanek, and J. S. Miller, Phys. Rev. B 18, 1673 (1978).
[26]R. J. Smith, J. Anderson, and G. J. Lapeyre, Phys. Rev. B 22, 632 (1980).
[27]J. W. Davenport, Chem. Phys. Lett. 77, 45 (1981).
[28]L. H. Little, *Infrared Spectra of Adsorbed Species* (Academic, London, 1966).
[29]O. Gunnarsson and K. Schönhammer, Phys. Rev. Lett. 41, 1608 (1978); 42, 195 (1979).
[30]P. S. Bagus, K. Hermann, and M. Seel, J. Vac. Sci. Technol. 18, 435 (1981).
[31]H. J. Freund and E. W. Plummer, Phys. Rev. B 23, 4859 (1981).
[32]R. P. Messmer, S. H. Lamson, and D. R. Salahub, Solid State Commun. 36, 265 (1980).
[33]A. Bianconi, M. Dell'Ariccia, P. J. Durham, and J. B. Pendry, Phys. Rev. B (in press).
[34]F. C. Brown, R. Z. Bachrach, and N. Lien, Nucl. Instrum. Methods 152, 73 (1978).
[35]J. Stöhr, R. Jaeger, J. Feldhaus, S. Brennan, D. Norman, and G. Apai, Appl. Opt. 19, 3911 (1980).
[36]C. Kunz, in *Optical Properties of Solids: New Developments,* edited by B. O. Seraphin (North-Holland, Amsertdam, 1976), p. 474.
[37]F. C. Brown and O. Rustgi, Phys. Rev. Lett. 28, 497 (1972).
[38]J. C. Fuggle and N. Martensson, J. Electron Spectrosc 21, 275 (1980); *Photoemission in Solids I and Photoemission in Solids II,* Vols. 26 and 27 of *Topics in Applied Physics,* edited by M. Cardona and L. Ley (Springer, Berlin, 1979), p. 373.
[39]D. Denley, P. Perfetti, R. S. Williams, D. A. Shirley, and J. Stöhr, Phys. Rev. B 21, 2267 (1980).
[40]W. E. Moddeman, T. A. Carlson, M. O. Krause, B. P. Pullen, W. E. Bull, and G. K. Schweitzer, J. Chem. Phys. 55, 2371 (1971).
[41]J. C. Fuggle, E. Umbach, R. Kakoschke, and D. Menzel, J. Electron Spectrosc. 26, 111 (1982).
[42]P. W. Palmberg, J. Electron. Spectrosc. 5, 691 (1974).
[43]P. R. Norton, R. L. Tapping, and J. W. Goodale, Chem. Phys. Lett. 41, 247 (1976); C. R. Brundle (private communication).
[44]C. R. Brundle, J. Vac. Sci. Technol. 13, 301 (1976).
[45]C. R. Brundle (private communication).
[46]A. Bianconi, R. Z. Bachrach, S. B. M. Hagström, and S. A. Flödstrom, Phys. Rev. B 19, 2837 (1979); 19, 3879 (1979).
[47]J. Stöhr, L. I. Johansson, S. Brennan, M. Hecht, and J. N. Miller, Phys. Rev. B 22, 4052 (1980).
[48]A. Bianconi, Surf. Sci. 89, 41 (1979); A. Bianconi and R. S. Bauer, *ibid* 99, 76 (1980).
[49]J. C. Fuggle, E. Umbach, D. Menzel, K. Wandelt, and C. R. Brundle, Solid State Commun. 27, 65 (1978).
[50]T. N. Rescigno and P. W. Langhoff Chem. Phys. Lett. 51, 65 (1977).
[51]N. Padial, G. Csanak, B. V. McKoy, and P. W. Langhoff, J. Chem. Phys. 69, 2992 (1978).
[52]W. Butscher, R. J. Buenker, and S. D. Peyerimhoff, Chem. Phys. Lett. 52, 449 (1977).
[53]S. Iwata, N. Kosugi, and O. Nomura, Jpn. J. Appl. Phys. 17, Suppl. 17-2, 105 (1978).
[54]S. Wallace, Ph.D. dissertation, Boston University, 1980 (unpublished); S. Wallace, D. Dill, and J. L. Dehmer, J. Chem. Phys. 76, 1217 (1982).
[55]R. S. Williams, D. Denley, D. A. Shirley, and J. Stöhr, J. Am. Chem. Soc. 102, 5718 (1980).
[56]D. W. Turner, A. D. Baker, C. Baker, and C. R. Brundle, *Molecular Photoelectron Spectroscopy* (Wiley, New York, 1970).
[57]M. Krauss and F. H. Mies, Phys. Rev. A 1, 1592 (1970).
[58]M. Tronc, G. C. King, R. C. Bradford, and F. H. Read, J. Phys. B 9, L555 (1976).
[59]M. Tronc, G. C. King, and F. H. Read, J. Phys. B 12, 137 (1979).
[60]E. Umbach, A. Schichl, and D. Menzel, Solid State Commun. 36, 93 (1980).
[61]P. S. Bagus, C. R. Brundle, K. Hermann, and D. Menzel, J. Electron Spectrosc. 20, 253 (1980).
[62]K. Herman, P. S. Bagus, C. R. Brundle, and D. Menzel (unpublished).
[63]K. H. Hillier and V. R. Saunders, Mol. Phys. 23, 1025 (1971).
[64]I. P. Batra and P. S. Bagus, Solid State Commun. 16, 1097 (1975).
[65]I. P. Batra and C. R. Brundle, Surf. Sci. 57, 12 (1976).
[66]H. Conrad, G. Ertl, J. Küppers, and E. E. Latta, Surf. Sci. 50, 296 (1975).
[67]H. P. Bonzel and G. Pirug, Surf. Sci. 62, 45 (1977).
[68]J. Kanski and T. N. Rhodin, Surf. Sci. 65, 63 (1977).

[69]H. Conrad, G. Ertl, J. Küppers, and E. E. Latta, Surf. Sci. 65, 235 (1977).
[70]E. Umbach, S. Kulkarni, P. Feulner, and D. Menzel, Surf. Sci. 88, 65 (1979).
[71]E. Umbach, Surf. Sci. 117, 482 (1982).
[72]C. R. Brundle, P. S. Bagus, D. Menzel, and K. Hermann (unpublished).
[73]R. Jaeger, J. Stöhr, and T. Kendelewicz (unpublished).
[74]K. Schönhammer and O. Gunnarsson, Solid State Commun. 23, 691 (1977); 26, 399 (1978); Z. Phys. B 30, 297 (1978); Phys. Rev. B 18, 6608 (1978).
[75]T. L. Brown and D. J. Darensbourg, Inorg. Chem. 6, 971 (1967).
[76]J. W. Davenport, Chem. Phys. Lett. 77, 45 (1981).
[77]G. Herzberg, *Spectra of Diatomic Molecules* (Van Nostrand, New York 1950).
[78]J. W. Davenport, J. Vac. Sci. Technol. 15, 433 (1978).
[79]J. C. Fuggle, M. Steinkilberg, and D. Menzel, Chem. Phys. 11, 307 (1975).
[80]R. J. Smith, J. Anderson, and G. J. Lapeyre, Phys. Rev. Lett. 37, 1081 (1976).
[81]G. Apai, P. S. Wehner, R. S. Williams, J. Stöhr, and D. A. Shirley, Phys. Rev. Lett. 37, 1497 (1976).
[82]P. M. Williams, P. Butcher, J. Wood, and K. Jacobi, Phys. Rev. B 14, 3215 (1976).
[83]J. Hermanson, Solid State Commun. 22, 9 (1977).
[84]G. J. Lapeyre, R. J. Smith, and J. Anderson, J. Vac. Sci. Technol. 14, 384 (1977); Surf. Sci. 89, 304 (1979); Phys. Rev. B 17, 2436 (1978).
[85]K. Horn, J. DiNardo, W. Eberhardt, H.-J. Freund, and E. W. Plummer, Surf. Sci. 118, 465 (1982).
[86]S. Wallace and D. Dill, Phys. Rev. B 17, 1692 (1978).
[87]D. Dill, J. R. Swanson, S. Wallace, and J. L. Dehmer, Phys. Rev. Lett. 45, 1393 (1980).
[88]S. P. Weeks and A. Liebsch, Surf. Sci. 62, 197 (1977).
[89]D. P. Woodruff, D. Norman, B. W. Holland, N. V. Smith, H. H. Farrel, and M. M. Traum, Phys. Rev. Lett. 41, 1130 (1978).
[90]L. G. Petersson, S. Kono, N. F. T. Hall, C. S. Fadley, and J. B. Pendry Phys. Rev. Lett. 42, 1545 (1979).
[91]J. Stöhr, in *Emission and Scattering Techniques,* edited by P. Day (Reidel, Dordrecht-Holland, 1981), p. 213.
[92]J. Stöhr, R. Jaeger, and S. Brennan, Surf. Sci. 117, 503 (1982).
[93]G. K. Green, BNL Report No. 50522, 1976, and BNL Report No. 50595, 1977, Vol. II (unpublished). Note that P is often defined as $(I_{||}-I_{\perp})/(I_{||}+I_{\perp})$ which is considerably smaller.
[94]N. V. Richardson and A. M. Bradshaw, Surf. Sci. 88, 255 (1979).
[95]G. Loubriel, Ph.D. dissertation, University of Pennsylvania, 1979 (unpublished).
[96]M. Passler, A. Ignatiev, F. Jona, D. W. Jepsen, and P. M. Marcus, Phys. Rev. Lett. 43, 360 (1979).
[97]S. Anderson and J. B. Pendry, Phys. Rev. Lett. 43, 363 (1979).
[98]S. Lehwald, J. T. Yates, Jr., and H. Ibach, in *Proceedings of the Fourth International Conference on Solid Surfaces, Cannes, France, 1980,* edited by D. A. Degras and M. Costa (Societé Francaise du Vide, Paris, 1980), Vol. II, p.221.
[99]H. Ibach and S. Lehwald, Surf. Sci. 76, 1 (1978).
[100]J. Stöhr and R. Jaeger (unpublished).
[101]C. R. Natoli, D. K. Misemer, S. Doniach, and F. W. Kutzler, Phys. Rev. A 22, 1104 (1980).
[102]P. J. Durham, J. B. Pendry, and C. H. Hodges, Solid State Commun. 38, 159 (1981).